THE JOURNAL OF PHYSICAL CHEMISTRY B

Article

pubs.acs.org/JPCB

Influence of Counterions on Lauric Acid Vesicles and Theoretical Consideration of Vesicle Stability

Wenlong Xu, Xiaolin Wang, Zhenhuan Zhong, Aixin Song, and Jingcheng Hao*

Key Laboratory of Colloid and Interface Chemistry, Shandong University, Ministry of Education, Jinan 250100, P. R. China

Supporting Information

ABSTRACT: The counterions, including inorganic cations, Na^+ and Cs^+, and organic cation, $(C_2H_5)_4N^+$, influence the phase behavior and self-assembled structures of the lauric acid (LA) in water. Dissolving LA in NaOH, CsOH, and $(C_2H_5)_4NOH$ (tetraethylammonium hydroxide, TeAOH) solutions, respectively, we observed that the three systems totally exhibited the same phase behavior, from birefringent L_α phase/precipitates (P) → L_α phase → L_α phase/L_1 (micelles) → L_1. The temperature influence on phase behavior was investigated, and with an increase of temperature, we observed that less phase behavior change occurred in the systems of LA/CsOH/H_2O and LA/TeAOH/H_2O, while the phase behavior of the LA/NaOH/H_2O system exhibited an obvious change. Cryogenic transmission electron microscopy (cryo-TEM) images demonstrated that the different microstructures of L_α phase samples in the three systems existed. For the systems of LA/NaOH/H_2O and LA/TeAOH/H_2O, uni- and multilamellar vesicles coexist for L_α phase samples, as both the morphology and size of these vesicles are polydisperse. The curvatures of the bilayer membranes of the two systems are considered to vary from positive, zero, and even negative. However, only spherically unilamellar vesicles exist in the system of LA/CsOH/H_2O, indicating that the bilayers are more rigid than those in the LA/NaOH/H_2O and LA/TeAOH/H_2O systems. Through the combination of the Helfrich curvature energy theory and the mass-action model, the effective bending constant $K = 0.5\ k_BT$ in the LA/CsOH/H_2O system was obtained, demonstrating that the unilamellar vesicles are stabilized by thermal fluctuations. A primary discussion for the effect of the nature of counterions on the stability and deformation of the vesicles is presented.

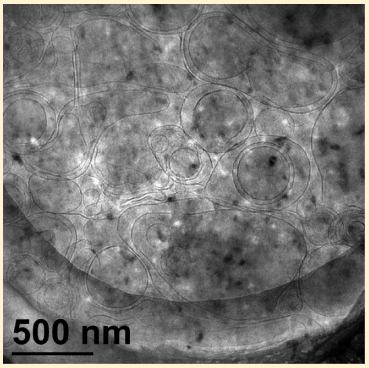

INTRODUCTION

Fatty acid vesicles produced from fatty acids and their soaps in aqueous solution are fascinating and valuable projects for both theoretical considerations and practical field studies. Fatty acids can be purified from plant oils and adipose tissue of animals.[1] Out of the perfect advantage of low toxicity and wide sources, fatty acids are the kind of natural green reagents to be widely used in cosmetic fields, and play an important role in the regulation of the composition of soil. The usual counterions of the fatty acid salts such as Na^+ for vesicles are monovalent cations.[2] Dissolving fatty acid in alkali solution with a certain ratio, the mixtures of fatty acid and their soap can be obtained and aggregates such as vesicles can be formed by titration.[3] These aggregates are stabilized by weak interactions such as electrostatic and hydrophobic interactions. Hydrogen bonds[4] were argued to be responsible for the formation of vesicles of fatty acids dissolved in alkali solutions. In general, fatty acid vesicles have come to people's attention, having become a hot topic and being widely used in different fields.

The first observation for fatty acid vesicles was in oleic acid and oleate mixtures in water by Gebicki,[5] in which an unsaturated fatty acid soap was used. After that, more and more fatty acid vesicles were produced in the mixtures of saturated fatty acids and their soaps. In 1988, Cistola[3] applied Gibbs phase rules to explain the ionization of the fatty acid soap at different temperatures and pointed out vesicles can be formed within a certain pH range, ca. 7−9. In 2007, Walde[6] reported vesicles from an unsaturated fatty acid soap, docosahexaenoic acid (DHA), in water. They also presented a review entitled "Fatty Acid Vesicles"[7] which summarized the literature works and discussed the features of fatty acid vesicles and the application as a protocell model. They also indicated more detailed studies are needed on fatty acid vesicles.

Herein, we investigated the differences of lauric acid (LA) vesicles from the reaction of LA with three kinds of alkali, NaOH, CsOH, and $(C_2H_5)_4NOH$. We observed the phase boundaries of the three systems at different temperatures and determined microstructures by cyro-TEM images. These systems were investigated for three reasons: (i) LA is an important compound in the cosmetics field, while the three alkalis are common in the laboratory. They play different roles in the formation of LA vesicles because of the different nature of their cations, e.g., ionic radius, extent of hydration, etc. (ii) NaOH and CsOH are inorganic alkalis, while $(C_2H_5)_4NOH$ is an organic alkali. As a result, the different influences from inorganic and organic alkalis can be obtained. (iii) The stability of fatty acid vesicles has been a controversial topic in recent years.[8,9] Through the size distribution of the LA−CsL mixture

Received: July 4, 2012
Revised: December 6, 2012
Published: December 11, 2012

   dx.doi.org/10.1021/jp306630n | J. Phys. Chem. B 2013, 117, 242−251

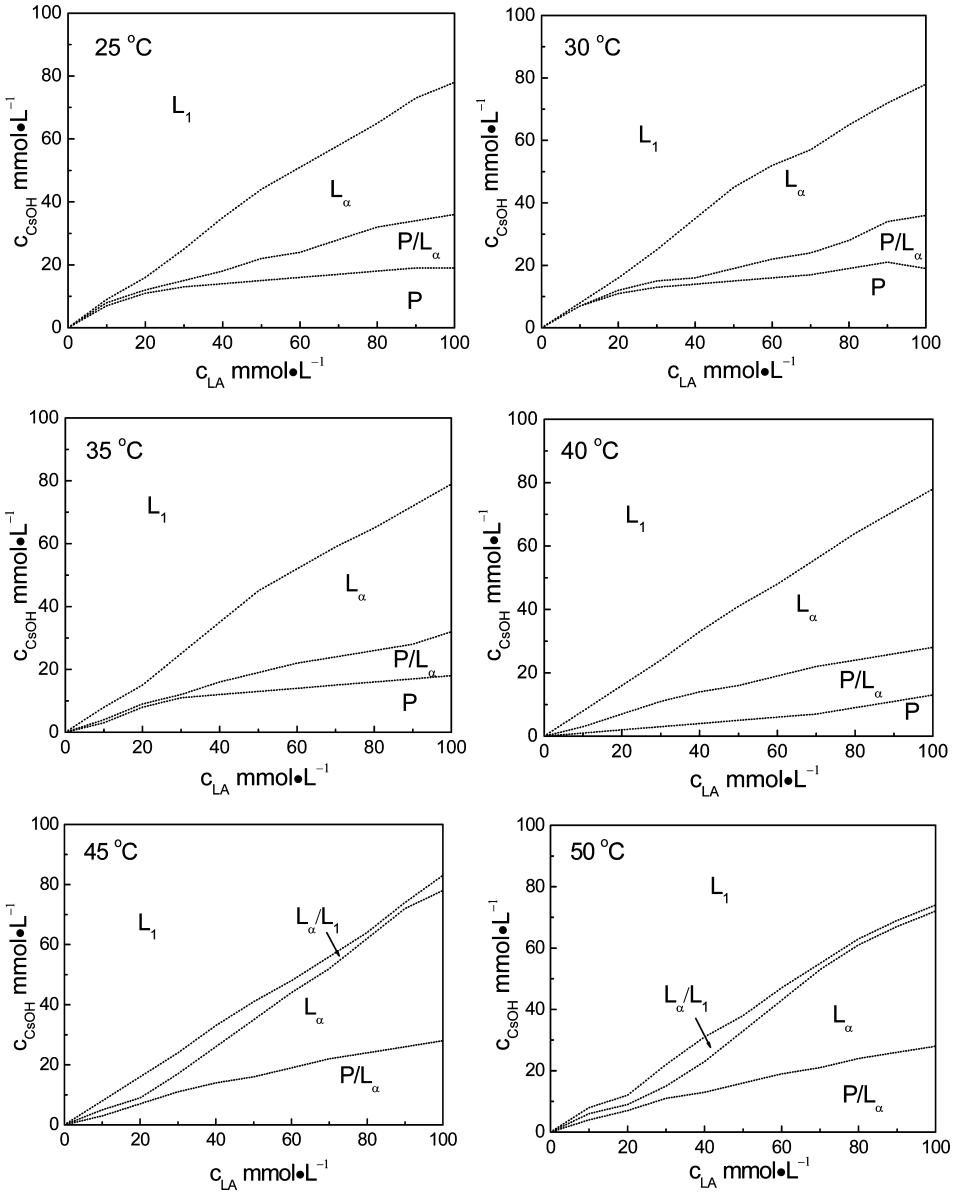

Figure 1. Phase boundaries of the LA/CsOH/H_2O system from 25 to 50 °C.

vesicles, we obtained the effective bending constant K of the LA/CsOH/H_2O system to prove their stability.

EXPERIMENTAL SECTION

Chemicals and Materials. Lauric acid was purchased from Fluka (>99%, mass fraction). Tetraethylammonium bromide (TeAB, >98%, mass fraction), NaOH (>98%, mass fraction), and CsOH (>99%, mass fraction) were purchased from J&K Scientific Co., Ltd. (China). KOH was purchased from Aladdin Chemistry Co., Ltd. Tetraethylammonium hydroxide (TeAOH) was prepared by an anion exchanger (Ion exchanger III, Merck) at room temperature. Bromide ions cannot be detected by $AgNO_3$ in the TeAOH stock solution ($Ag^+ + Br^- \rightarrow AgBr\downarrow$), so the ion exchange with hydroxide is >99%. The water used was ultrapure water with a resistivity of 18.25 MΩ·cm from a UPH-IV ultrapure water purifier (China). The other reagents were analytical grade.

Phase Behavior Study. The mixtures were established by dissolving LA in different alkali solutions, NaOH, CsOH, and TeAOH, at different ratios (r = LA/NaOH, LA/CsOH, or LA/TeAOH), respectively. The mixtures were heated to 50 °C in an ultrasonic instrument for 2 h. After that, the mixtures were put into a thermostatic water bath to equilibrate at least for 2 weeks at 50 °C. The phase boundary was established by visual inspection with the help of crossed polarizers. The phase boundaries were confirmed through the data of pH and conductivity. The samples were equilibrated at T = 45, 40, 35, 30, and 25 °C, respectively, for 2 weeks. The phase boundaries at different temperatures can be obtained.

Conductivity and pH Measurements. The conductivity measurements were performed on a DDSJ-308A (China) conductivity meter with a DJS-1C glass electrode at 40.0 ± 0.1 °C. The values of pH were determined on a PHS-3C pH meter (China) with an E-201-C glass electrode at 40.0 ± 0.1 °C. The two-phase samples were detected under stirring.

Polarization Optical Microscopy Observations (POM). The textures of L_α phase samples were characterized on a Carl Zeiss Axioskop 40 light microscope (Jena, Germany). Two crossed polarizers were applied for the observations.

dx.doi.org/10.1021/jp306630n | J. Phys. Chem. B 2013, 117, 242−251

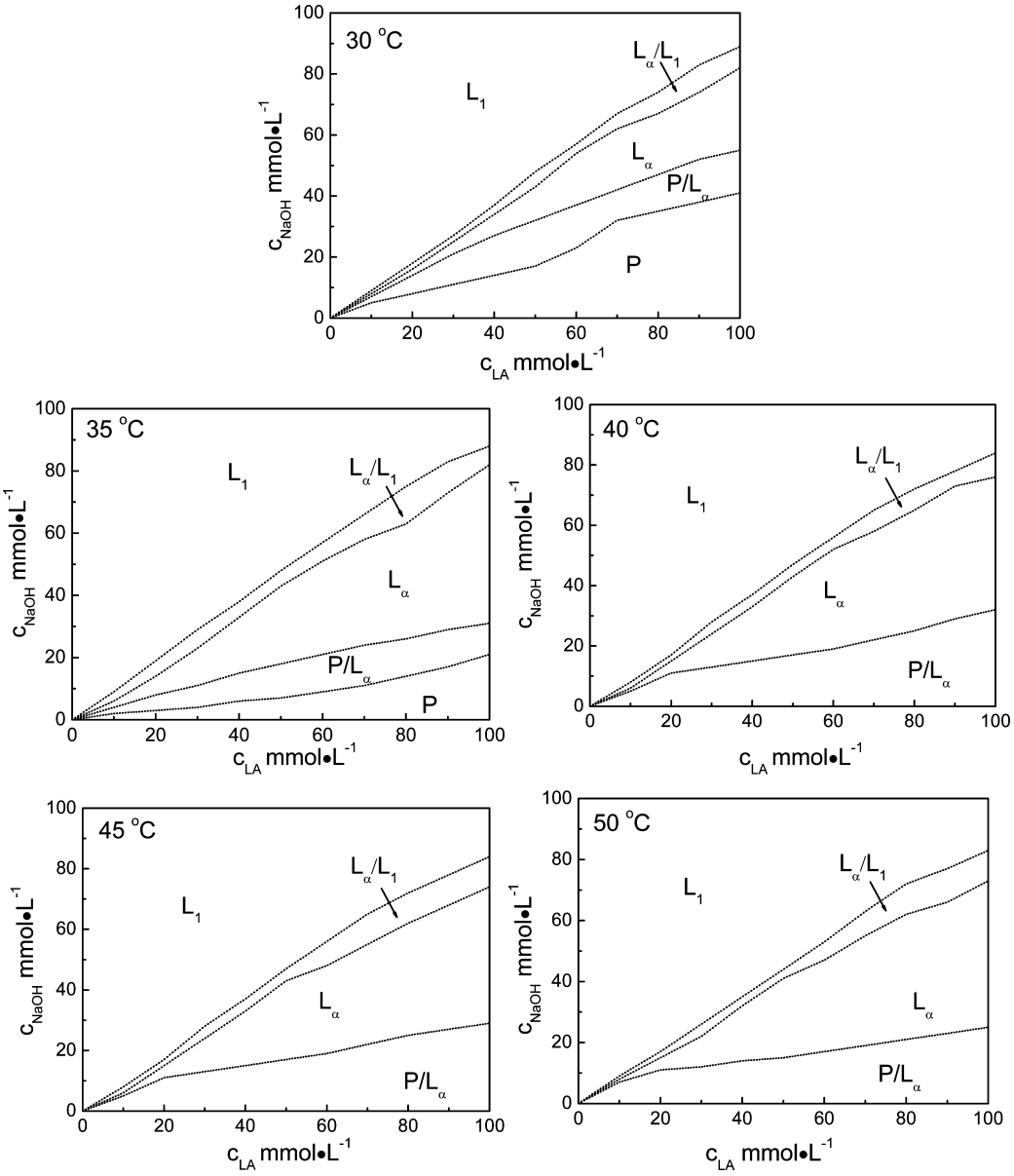

Figure 2. Phase boundaries of the LA/NaOH/H_2O system from 25 to 50 °C. The phase boundary of the LA/NaOH/H_2O system at 25 °C was not shown because the L_α phase was not obtained.

Differential Scanning Calorimetry (DSC) Measurements. The phase transition temperature was measured on a DSC-Q10 (TA Instruments, New Castle, PA). The measuring range of temperature was from 25 to 50 °C at a rate of 3 °C/min.

Cryogenic Transmission Electron Microscopy (cryo-TEM) Observations. A drop of sample solution (~4 μL) was dropped on a microgrid in a high humidity environment (>90%). The excess sample was blotted up by two pieces of blotting paper, leaving a thin film sprawled on the microgrid. The microgrid was then plunged into liquid ethane which was then frozen by liquid nitrogen. The vitrified sample was transferred into a sample holder (Gatan 626) and inserted into a TEM (JEOL JEM-1400 TEM operated at 120 kV). The images were recorded on a Gatan multiscan CCD. During the process, the temperature was controlled lower than −165 °C.

Dynamic Light Scattering (DLS) Measurements. DLS measurements were performed on a dynamic light scatting instrument (BI-200SM, Brookhaven, England). The incident light was a laser at 488 nm, and the incident angle was 90°. The data measured by DLS were analyzed through the method of CONTIN, and a size distribution diagram in the weight of light intensity was obtained.

RESULTS AND DISCUSSION

Phase Behavior. The phase boundaries of the three systems, LA/NaOH/H_2O, LA/CsOH/H_2O, and LA/TeAOH/H_2O, were obtained at T = 25, 30, 35, 40, 45, and 50 °C. Figures 1 and 2 show the typical phase boundaries of the LA/CsOH/H_2O and LA/NaOH/H_2O systems at different temperatures. The phase boundaries of the LA/TeAOH/H_2O system are shown in Figure S1 (Supporting Information). More than 100 samples were prepared to control the relative errors of the phase boundaries for every system. The phase transition was a gradual process with the change of concentration; as a result, the phase transition boundaries were ambiguous and we

dx.doi.org/10.1021/jp306630n | J. Phys. Chem. B 2013, 117, 242−251

used dotted lines to signify them. Phase separation (not shown in the phase boundaries) occurred when the total concentration of surfactant was very low, which is a common phenomenon in ionic surfactant systems.[10] It is assumed that the neutralization reaction occurs as shown below.

$$C_{11}H_{23}COOH + (Na, Cs, or TeA)OH \rightarrow C_{11}H_{23}COO(Na, Cs, or TeA) + H_2O$$

One can see that the phase transition tendencies of the three systems are almost the same; when r_{LA/OH^-} = 1:1, L_1 is obtained for the three systems. With an increase of r, L_α/L_1, L_α, and L_α/P phase regions occur. The Krafft point of sodium laurate has been reported by several groups; the values are inconsistent from 21 to 44 °C.[11−13] Herein, the sample is transparent L_1 at r = 1:1 of 25 °C, meaning the Krafft point should be lower than 25 °C.

We calculated the area percentages of the L_α phase in the phase boundaries, which was shown in Figure 3 as a function of

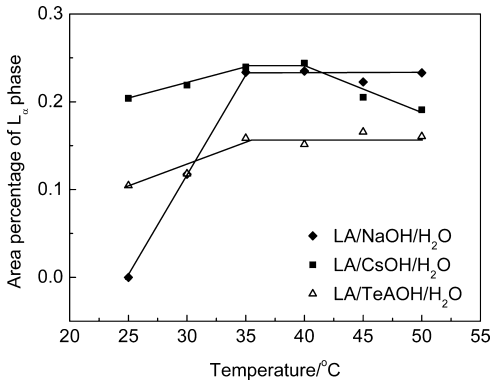

Figure 3. Area percentage of the L_α phase of the three systems from 25 to 50 °C. The relative errors of the L_α area percentages which were calculated from more than 100 samples of each system are ±10%.

temperature. One can see, with the increase of temperature, the area percentages of the L_α phase region initially change larger for the three systems. When it comes to 35−40 °C, the area percentages of the L_α phase keep constant. However, above 40 °C, for the LA/CsOH/H_2O system, the area percentage of the L_α phase changes lower, while the other two systems of LA/NaOH/H_2O and LA/TeAOH/H_2O keep constant. For inorganic alkalis, NaOH and CsOH, the two systems of LA/NaOH/H_2O and LA/CsOH/H_2O do not show similar features of L_α phase area with temperature; however, similar features of L_α phase area with temperature can be observed for LA/NaOH/H_2O and LA/TeAOH/H_2O. This means different counterions have little influence on the phase behavior but have a great influence with the increase of temperature.

To explain the phenomenon, we measured the phase transition temperature for the three systems at a certain concentration. From Figure 4, we detected an endothermic peak at T = ~33.92 °C for the LA/NaOH/H_2O system, while the other two systems did not have a peak, indicating a phase transition occurred in the LA/NaOH/H_2O system at about 33.92 °C, while no phase transition occurred in the other two systems. These results are consistent with our phase boundaries. Hargreaves et al.[2] reported the melting points of anhydrous fatty acids and crystals in water. For sodium laurate, the melting point of anhydrous fatty acid is about 42 °C, while

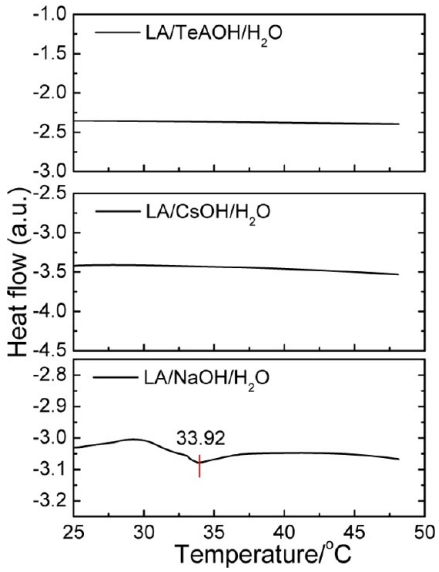

Figure 4. Phase transition temperature measured by DSC. The three samples were chosen at the same concentration. c_{LA} = 100 mmol·L^{-1} and c_{OH^-} = 40 mmol·L^{-1}.

that of crystals in water is about 33 °C, which is consistent with our results. The transition between the L_α phase and crystal phase is reversible. According to the analysis, we can conclude that different counterions have a great effect on the Krafft point of laurate. A counterion with larger radius decreases the Krafft point more effectively.

Typical sample photographs of the LA/NaOH/H_2O system at 40 °C were prepared with c_{LA} = 100 mmol·L^{-1} but varying the NaOH concentration gradually. From Figure 5, one can see

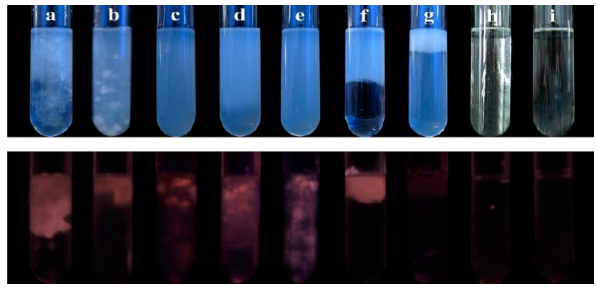

Figure 5. Typical sample photographs of the LA/NaOH/H_2O system at 40 °C without (top) and with (bottom) polarizers. c_{LA} = 100 mmol·L^{-1} with varying NaOH concentration gradually. From left to right: 20 (a), 30 (b), 40 (c), 50 (d), 60 (e), 70 (f), 80 (g), 90 (h), and 100 mmol·L^{-1} (i). The solution volume was fixed at 5 mL.

the tendency of the phase transition, $L_\alpha/P \rightarrow L_\alpha \rightarrow L_\alpha/L_1 \rightarrow L_1$. The L_α phase samples are bluish solutions with birefringent textures in the crossed polarizers. Cross-like spherulite textures were detected in the polarized optical microphotos, as shown in Figure 6, for a typical POM image of the LA/NaOH/H_2O system (Figure S2, Supporting Information, LA/CsOH/H_2O and LA/TeAOH/H_2O systems), meaning the existence of lamellar structures. L_1 phase samples are isotropic solutions. When the concentration of NaOH reached 40 mmol·L^{-1}, that is, r = 100:40, a homogeneous phase occurred, which means the excess LA was solubilized into the NaL micellar solution. In this case, the composition is 60 mmol·L^{-1} LA and 40 mmol·L^{-1} NaL. When r = 1:1, a L_1 phase was observed and NaL micellar

dx.doi.org/10.1021/jp306630n | J. Phys. Chem. B 2013, 117, 242−251

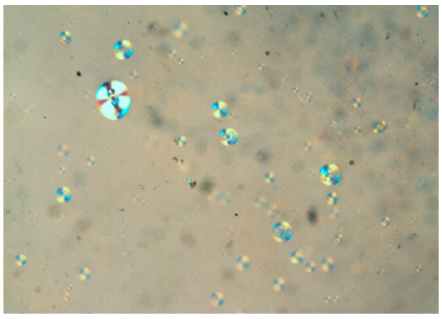

Figure 6. A typical polarized optical micrograph at 40 °C for an L_α sample in the LA/NaOH/H_2O system. c_{LA} = 100 mmol·L^{-1} and c_{NaOH} = 40 mmol·L^{-1}.

solution was formed. At $r \ll 1$, that is, the concentration of NaOH is the larger than that of LA, a gel phase was detected, which was reported in our previous work.[14]

The changes of conductivity and pH for the three systems were measured at 40 °C. From Figure 7, we can conclude that the two systems of LA/NaOH/H_2O and LA/CsOH/H_2O have a similar pH value range (~7−9) in the L_α phase region. A similar system was reported by Hargreaves,[2] which is accordant with our results. However, the LA/TeAOH/H_2O system has a narrow pH value range (~7.50−8.20) because of a narrow L_α phase region. This may be because TeAOH has a larger polar head, resulting in a lower value of p (packing parameter, elaborated in the Discussion part). As a result, a narrow L_α phase region is observed. These results of the three systems are totally consistent with the literature.[3]

The tendency of conductivity changes is similar in the three systems. With the increase of alkalis, κ increases initially and increases promptly at high alkali concentration. In the L_α phase, one would suspect that the free ions were trapped in the inner water cores of the L_α phase which are vesicles determined by cryo-TEM observations.

Microstructures of the L_α Phase. We determined the microstructures of the L_α phase by the cryo-TEM observations. From Figure 8, one can clearly see that the L_α phase contains vesicles in the four systems of LA/NaOH/H_2O, LA/KOH/H_2O, LA/CsOH/H_2O, and LA/TeAOH/H_2O. In order to analyze the effect of the nature of counterions, i.e., ionic radius, extent of hydration, etc., on the stability of the vesicles, the L_α phase of the system LA/KOH/H_2O was also studied by cryo-TEM. It is also seen that the morphologies and size of the vesicles for LA/CsOH/H_2O differ from those of the other three systems of LA/NaOH/H_2O, LA/KOH/H_2O, and LA/TeAOH/H_2O. Vesicles of LA/CsOH/H_2O are almost unilamellar and spherical (Figure 8a) but display polydispersity in size, while those of the other three systems are rather polydisperse both in size and morphologies, with unilamellar vesicles, multilamellar vesicles, and olig-vesicles coexisting. Obvious deformation of vesicles can be observed in the systems LA/NaOH/H_2O, LA/KOH/H_2O, and LA/TeAOH/H_2O. These vesicles should have a low rigidity, which are common in the hydrocarbon surfactants.[15−17] Moreover, one can see both uni- and multilamellar vesicles in the images of Figure 8b and c for the two systems LA/NaOH/H_2O and LA/KOH/H_2O with the counterions of inorganic ions and images of Figure 8d and e for the system LA/TeAOH/H_2O having the counterions of organic ions. These vesicles are irregular both in shape and size. Some multilamellar vesicles share the same outer bilayer with other vesicles; that is, olig-vesicles exist (indicated by the white arrows in Figure 8d to e). The radii of the vesicles are in the range 20−400 nm. Different kinds of bilayer structures occur in a single phase, meaning a very low value of mean bending constant κ.[18−20] However, only unilamellar spherical vesicles exist in the system of LA/

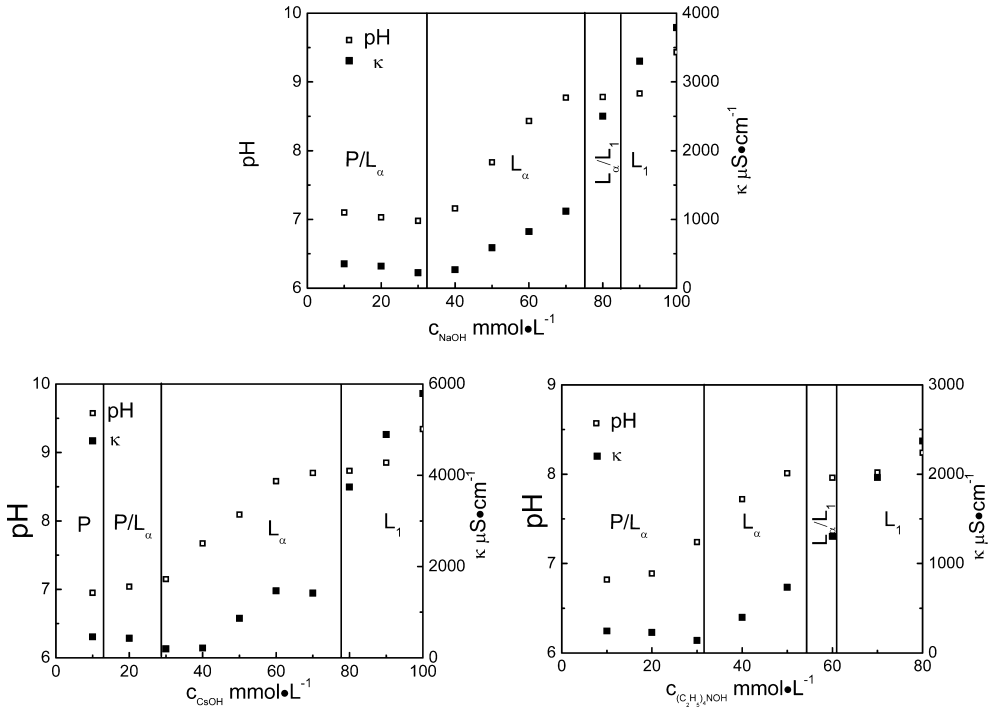

Figure 7. A section of phase boundaries of the three systems at 40 °C. c_{LA} = 100 mmol·L^{-1}. The data of conductivity (κ) and pH were given in the boundaries.

dx.doi.org/10.1021/jp306630n | J. Phys. Chem. B 2013, 117, 242−251

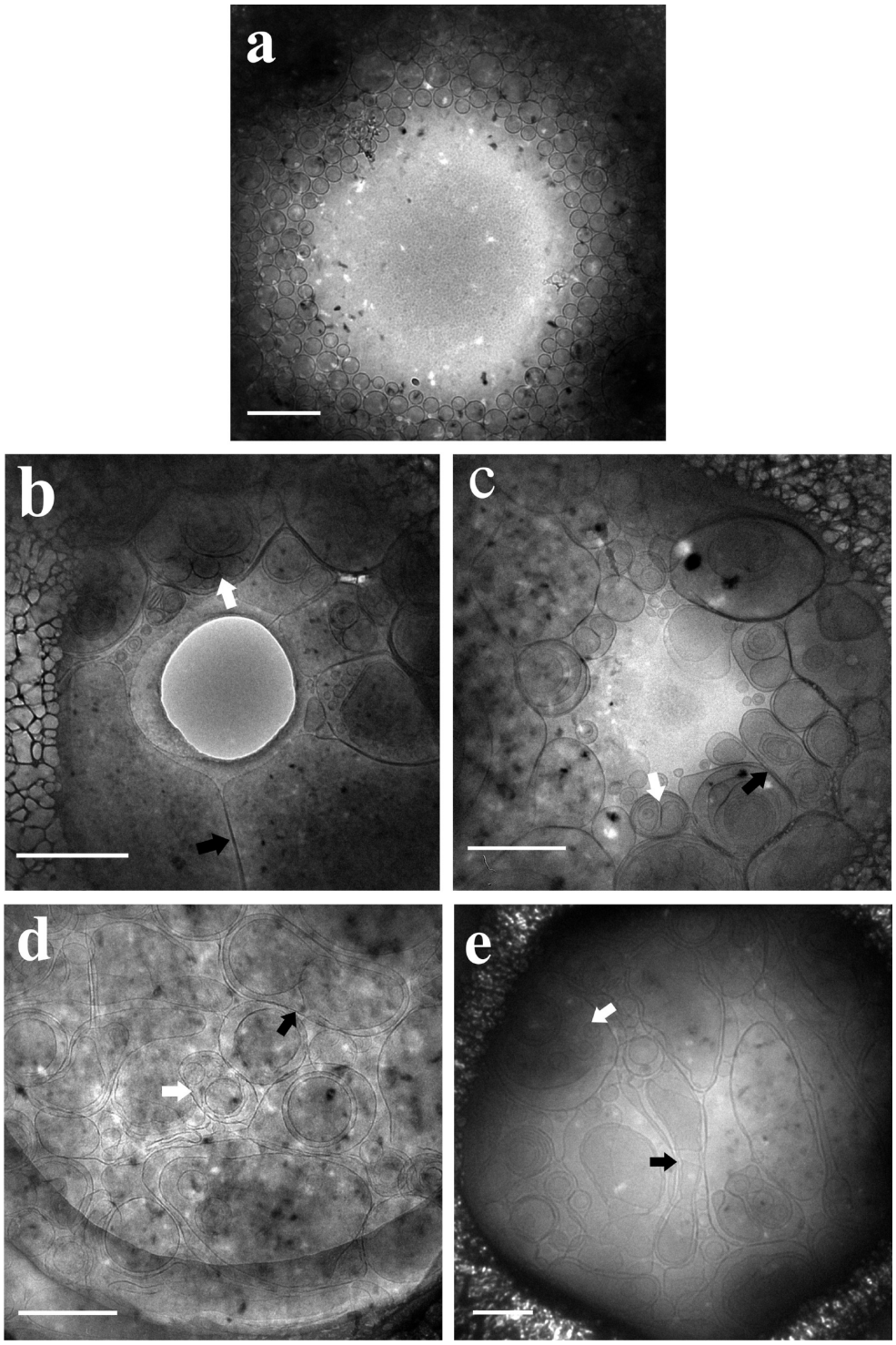

Figure 8. Cryo-TEM images of the systems at 40 °C. LA/CsOH/H_2O (a), LA/NaOH/H_2O (b), LA/KOH/H_2O (c), and LA/TeAOH/H_2O (d and e). The black arrows indicate the curvature equal to zero or negative, and the white arrows indicate olig-vesicles. Scale bar = 500 nm. c_{LA} = 100 mmol·L^{-1}, c_{OH^-} = 40 mmol·L^{-1}.

CsOH/H_2O, indicating that the bilayers formed by Cs^+ are more rigid than other counterions. As a result, we conclude that only Cs^+ has a rigidity to keep the vesicles spherical but organic ion, TeA^+, has a similar property to inorganic ions, Na^+ and K^+, to produce irregular vesicles both in shape and size.

One can observe the curvature of bilayer membranes, which should be different from place to place. The curvatures indicated by the black arrows in Figure 8 are equal to zero or even negative. In general, spontaneous curvature c_0 is equal to zero only when there is a composition symmetry between the inner and outer monolayers of the surfactant bilayer membranes; otherwise, $c_0 \neq 0$.[21−23] For these systems, the rigidity of the surfactant aggregates is very low and deformation occurs in which the vesicles stack compactly. As a result, planar lamellar structures exist. When the repulsion interaction between bilayers increases, negative curvature occurs. As

dx.doi.org/10.1021/jp306630n | J. Phys. Chem. B 2013, 117, 242−251

shown in Figure 9, if the composition of the bilayer membranes is coincident, $c_0 = 0$, if the surfactant area of the outer layer is larger than the inner layer, $c_0 > 0$, and otherwise, $c_0 < 0$.

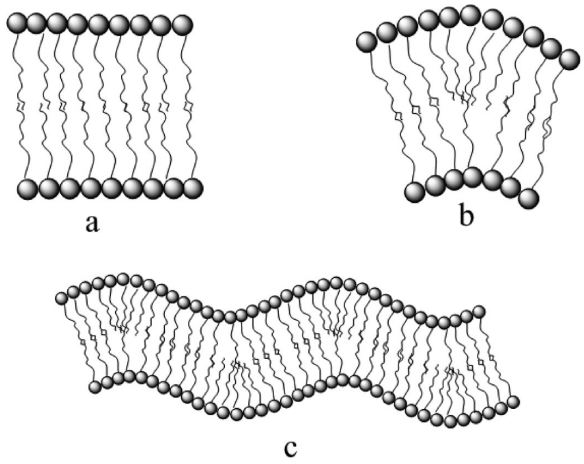

Figure 9. Schematic illustration of bilayer membranes with different curvatures: $c_0 = 0$ (a), $c_0 > 0$ (b), $c_0 > 0$ and $c_0 < 0$ coexist (c).

To explain the size distribution and the stability of vesicles, we introduced the theory of Helfrich curvature energy. According to Helfrich,[24] if the thickness (~6 nm) and the Debye length of the bilayers are much smaller than the radius,[20,25−27] the free energy per unit area of bilayer membranes, f_c, is

$$f_c = \frac{1}{2}\kappa\left(\frac{1}{R_1} + \frac{1}{R_2} - \frac{2}{r_0}\right)^2 + \bar{\kappa}\left(\frac{1}{R_1 R_2}\right) \quad (1)$$

where R_1 and R_2 are the principal curvature radii, r_0 is the spontaneous curvature radius, κ is the curvature modulus (mean bending constant), and $\bar{\kappa}$ is the saddle-splay modulus (Gaussian bending constant).

For spherical vesicles, $R_1 = R_2 = R$, eq 1 can be simplified

$$f = 2K\left(\frac{1}{R} - \frac{1}{R_0}\right)^2$$
$$2K = 2\kappa + \bar{\kappa}$$
$$R_0 = \frac{2\kappa + \bar{\kappa}}{2\kappa} r_0 \quad (2)$$

R_0 is the radius of the minimum curvature energy vesicles, and K is the effective bending constant. In these formulas, κ reflects the energy deviating from the spontaneous curvature. It controls the rigidity of the bilayers. If κ is the same order of magnitude with k_BT, the energy of Helfrich fluctuation is higher than that of curvature fluctuation. As a result, repulsion exists between the bilayers in short distance, which stabilizes the unilamellar vesicles. $\bar{\kappa}$ reflects the extent of saddle deformation. It controls the structure of the bilayers, which is a concept of topology and does not affect the size of vesicles. K is the sum of κ and $\bar{\kappa}$. If K is the same order of magnitude with k_BT, vesicles are stabilized by thermal fluctuation with a broad size distribution. On the other hand, if $K \gg k_BT$, vesicles are stabilized by spontaneous curvature with a narrow size distribution.[28]

For the systems of LA/NaOH/H_2O and LA/TeAOH/H_2O, vesicles are polydisperse both in morphology and size, the value of κ and K can be inferred to be very low, and $|\bar{\kappa}|$ should be high because of the significant deformation of vesicles. For the system of LA/CsOH/H_2O, vesicles are spherical and polydisperse in size, indicating a low $|\bar{\kappa}|$. However, we cannot determine κ and K directly.

As we can see from Figure 8a, the vesicles are unilamellar and spherical. An issue followed closely is whether the vesicles are stable or at a metastable station which can transform into multilamellar vesicles or even onion phase with many bilayers. To the best of our knowledge, the prerequisite of stable existence for unilamellar vesicles is that repulsion interactions must be higher than attraction interactions between bilayers.[29] Two mechanisms are usually applied to explain the stability of unilamellar vesicles: (i) Thermal fluctuation induces the repulsive interaction overcoming the attractive interaction ($\kappa \sim k_BT$).[20] (ii) Curvature energy from spontaneous curvature prohibits the occurrence of multilamellar vesicles.[20−22,25]

In fact, the equilibrium size distribution depends on the competition between mixing entropy and the curvature elasticity of the bilayers.[30−32] Connecting the size distribution histogram and theory model, the value of K can be obtained. When the size distribution is narrow, that is, $K \gg k_BT$, a simplified formula can be used.[28,33]

$$K = \left(\frac{k_BT}{16\pi}\right)\left(\frac{R_0}{\sigma}\right)^2 \quad (3)$$

Herein, R_0, the radius of the minimum curvature energy, can be approximately equal to the average radius, and σ is the standard deviation. However, in general, K is the order of magnitude with k_BT for the hydrocarbon surfactant aggregates. In this case, K can be obtained by fitting the size distribution histogram and mass-action model.[20,28,34]

$$\frac{X_N}{N} = \left\{\frac{X_M}{M}\exp\left[\frac{M(\mu_M^0 - \mu_N^0)}{k_BT}\right]\right\}^{N/M} \quad (4)$$

M is the distribution of surfactant between vesicles of aggregation number, corresponding to the minimum curvature energy radius, R_0, and N is the distribution of surfactant between vesicles of aggregation number, corresponding to radius R. X_M, μ_N^0 and X_N, μ_N^0 are the mole fraction of surfactant and the standard chemical potential per molecule in vesicles of size M and N, respectively. The standard chemical potentials of different vesicles are not equal because of the different curvature energies. As a result,

$$\mu_N^0 - \mu_M^0 = \frac{4\pi R^2 f}{N} = \frac{8\pi K\left(1 - \frac{R}{R_0}\right)^2}{N} \quad (5)$$

We define the average area of a single surfactant molecular as A_0, then

$$M = 8\pi {R_0}^2/A_0$$
$$N = 8\pi R^2/A_0 \quad (6)$$

If we insert eq 5 and eq 6 into eq 4, a function of size distribution can be obtained:

$$C_N = \left\{C_M \exp\left[\frac{-8\pi K}{k_BT}\left(1 - \frac{R_0}{R}\right)^2\right]\right\}^{R^2/{R_0}^2} \quad (7)$$

dx.doi.org/10.1021/jp306630n | J. Phys. Chem. B 2013, 117, 242−251

C_M (=X_M/M) and C_N (=X_N/N) are the number fractions of vesicles of size M and N, respectively.

There are several methods to determine the size distribution of vesicles. The most common one is dynamic light scattering (DLS) measurements. The hydrodynamic radius, R_h, can be obtained through the calculation of CONTIN. Characterizing promptly is a great advantage for this method. However, only dilute solution can be used in the method, and also because of the disturbance of some larger particles, R_h is usually larger than the actual radius in the weight of light intensity.[34] Another common method is to measure the radii of the vesicles in the cryo-TEM images and obtain a size distribution histogram by the statistic analysis method.[20,28,35] The radii of vesicles obtained in this way are almost equal to the actual ones, while this method is expensive and a waste of time. A convincing result can be obtained by the connection of the two methods.

We can determine the relationship between the results from DLS measurements and actual ones. The scattering intensity from a vesicle with the weight, M_i, is proportional to M_i^2, as a result, the z-average diffusion coefficient, D_z, as

$$D_z = \frac{\sum_i x_i M_i^2 D_i}{\sum_i x_i M_i^2} \tag{8}$$

x_i is the number fraction of size i, M_i is the mass of size i, and D_i is the diffusivity of size i. Because the structure of a vesicle is hollow, M_i is proportional to R_i^2, the radius of vesicle. As a result,

$$D_z = \frac{\sum_i x_i R_i^4 D_i}{\sum_i x_i R_i^4} \tag{9}$$

If we insert the Stokes−Einstein relation, $D_i = k_B T/(6\pi\mu R_i)$, into eq 9, we have

$$D_z = \frac{k_B T}{6\pi\mu} \frac{\sum_i x_i R_i^3}{\sum_i x_i R_i^4} \tag{10}$$

If we insert the Stokes−Einstein relation again, $R_h = k_B T/(6\pi\mu D_z)$, into eq 10, we can determine the average hydrodynamic radius

$$\langle R_h \rangle = \frac{\sum_i x_i R_i^4}{\sum_i x_i R_i^3} \tag{11}$$

We can obtain R_i and x_i from the size distribution histogram measured by cryo-TEM images.

The sample was measured three times to guarantee the accuracy of the results at 40 °C. As shown in Figure 10, the average hydrodynamic radii ($\langle R_h \rangle$ = 91.30 nm) determined by CONTIN are perfectly consistent for the three times measured. We measured the radii of about 3000 vesicles in the cryo-TEM images, and a size distribution histogram was obtained. We can see that most radii are in the range 40−80 nm and the average radius is about 63 ± 20 nm. Extract R_i and x_i from Figure 11, and according to eq 11, the theoretical average radius $\langle R_h \rangle$ determined by DLS can be calculated to be 91.04 nm, which is remarkably consistent with the practical data (91.30 nm) by the statistical method.

In order to determine the stability of the vesicles, we applied a curvilinear equation to fit the size distribution histogram (indicated by the red curve). K (=0.5 $k_B T$) can be determined through the comparison between the curvilinear equation and

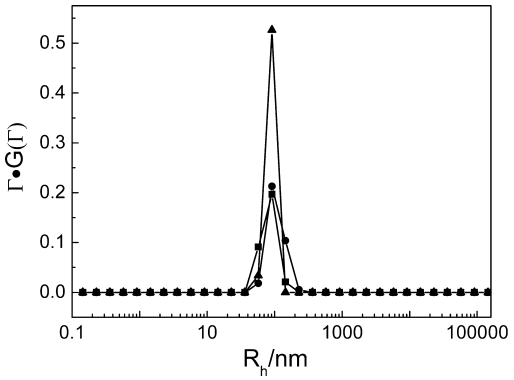

Figure 10. Size distribution diagram determined by DLS measurements at 40 °C. The average hydrodynamic radius is 91.30 nm.

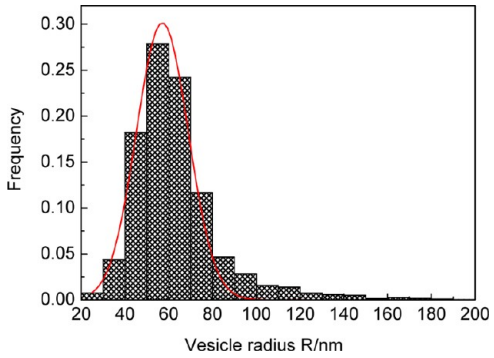

Figure 11. Vesicle size distribution histogram through the method of statistic analysis. The average radius is 63.12 ± 20.07 nm.

the theory equation (eq 7). As we referred to just now, when $K \sim k_B T$, vesicles are stabilized by Helfrich fluctuation with a broad size distribution, which is consistent with our histogram (20−200 nm). Within the method, κ and $\bar{\kappa}$ cannot be obtained.[28] CTAB/FC_7 is one of a few systems where the value of κ and $\bar{\kappa}$ can be measured.[36] In this system, flat discs coexist with spherical unilamellar vesicles, that is, $12\kappa \cong 8\pi\bar{\kappa}$. The effective bending constant $K = \kappa + \bar{\kappa}/2 = 6\ k_B T$ can be obtained through analyzing size distribution. As a result, $\kappa = (5 \pm 1)\ k_B T$ and $\bar{\kappa} = (2 \pm 1)\ k_B T$ were given. However, in our systems, only unilamellar vesicles exist and the accurate value of κ and $\bar{\kappa}$ cannot be determined. As we have referred, the value of $|\bar{\kappa}|$ is very low because of the spherical vesicles and according to $K = \kappa + \bar{\kappa}/2$ and $K = 0.5\ k_B T$, no matter if $\bar{\kappa} > 0$ or $\bar{\kappa} < 0$, κ is the order of magnitude with $k_B T$. Therefore, the thermal fluctuation repulsion energy is higher than the attractive interaction between the bilayer, which stabilized the unilamellar vesicles.

There must be some weak interactions to induce the formation of vesicles. In the fatty acid vesicles, the most important weak interaction is the hydrogen bond.[4,37−39] According to Israelachvili,[30] the differences among the surfactant aggregates result from the different styles the surfactant molecules stack. Through the packing parameter, p, we can connect the structure and the size of the surfactant molecules.

$$p = v/(la_0) \tag{12}$$

Herein, v and l are the volume and length of the hydrophobic chain and a_0 is the area of the hydrophilic groups of amphiphilic molecules. With the increase of p value, spherical micelles ($p \leq$

dx.doi.org/10.1021/jp306630n | J. Phys. Chem. B 2013, 117, 242−251

1/3), rod micelles or wormlike micelles ($1/3 < p < 1/2$), bilayers ($1/2 < p < 1$), and reverse structures ($p > 1$) occur in the solution gradually. The formation of hydrogen bonds makes the arrangement of surfactant hydrophilic groups more close, which reduce the value of a_0. According to eq 12, with no change of ν and l, p will increase when a_0 decreases. As a result, the probability of vesicle formation increases.

The structure of hydrogen bonds in fatty acid vesicles has been reported by many scientists, as Figure 12 shows.[39]

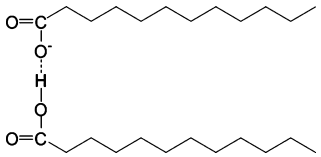

Figure 12. Schematic illustration of the hydrogen bond between LA and its salt which should be responsible for the formation of lauric acid vesicles.

The primary reason for fatty acid vesicle formation is no doubt hydrogen bonds among the fatty acid and its soap molecules; of course, the other weak interactions include electrostatic forces and hydrophobic interactions. It has been observed that, when the pH is at the pK_a of the fatty acid,[2,4,37] the pK_a value of LA has been reported as 7.5,[40] vesicles are easy to form, which is consistent with the data in Figure 7. The nature of counterions, such as hydrated radius and extent of hydration, on the phase behavior and the stability of the fatty acid vesicles should be considered. The concentration distribution of the counterions near the bilayers can affect the vesicles. The morphology and the size of vesicles are influenced when the counterion changes. Only unilamelar and spherical bilayer vesicles form in the system LA/CsOH/H_2O, indicating that the bilayers formed by Cs^+ are more rigid because the counterion, Cs^+, has the smaller hydrated radius (3.29 Å) compared to Na^+ (3.58 Å) and K^+ (331 Å).[41] Unilamellar, multilamellar, and olig-vesicles coexist in the two systems LA/NaOH/H_2O and LA/KOH/H_2O, in which the counterions, Na^+ and K^+, have a larger hydrated radius than that of Cs^+ ($Na^+ \gg K^+ > Cs^+$).[41] A smaller hydrated radius means weaker interaction between Cs^+ and H_2O, and a relatively stronger interaction between Cs^+ and the polar headgroup of L^-, which strengthens the rigidity of the bilayers. Considering the balance of the hydrophobicity, the density, and the hydrated radius (4.00 Å)[41] of the organic counterion, $(C_2H_5)_4N^+$, the morphology of vesicles in the system LA/TeAOH/H_2O deforms largely entirely as the other inorganic systems. Interestingly, with a decrease of hydrated radii of counterions but leaving out of consideration of inorganic or organic cations, one can observe the tendency from polydispersity to monodispersity and from deformed to spherical vesicles.

CONCLUSIONS

In conclusion, the fatty acid vesicle is the most common structure among fatty acid aggregates, and is easy to form at the range near pK_a. In our present systems, three fatty acid vesicle systems (LA/NaOH/H_2O, LA/CsOH/H_2O, and LA/TeAOH/H_2O) were characterized by the technique of DLS, cryo-TEM, etc. Phase transition occurred with the change of the surfactant ratio and concentration. Different phenomena were observed with different counterions. In mechanism, there is a change of packing parameter induced by the weak interactions, mainly by hydrogen bonds, hydrophobic interactions, and electric interactions. The microstructures of vesicles were given by cryo-TEM, indicating the higher rigidity of the vesicles formed by Cs^+. On the other hand, size distribution was determined in the method of statistic analysis and DLS measurements, which showed perfectly consistent. Through analyzing the size distribution histogram, the effective bending constant K was calculated directly and the curvature modulus κ and the saddle-splay modulus $\bar{\kappa}$ were estimated. As a result, the stability of vesicles was determined. Considering the importance in the field of cell models and drug delivery, etc., the study of fatty acid vesicles has a good application prospect, and we expect this paper can make some contributions to the development of fatty acid vesicles.

ASSOCIATED CONTENT

Supporting Information

Phase boundaries of LA/TeAOH/H_2O from 25 to 50 °C and polarized optical microphotos at 40 °C for the LA/CsOH/H_2O and LA/TeAOH/H_2O systems. This material is available free of charge via the Internet at http://pubs.acs.org.

AUTHOR INFORMATION

Corresponding Author

*Phone: +86-531-88366074. Fax: +86-531-88564750. E-mail: jhao@sdu.edu.cn.

Notes

The authors declare no competing financial interest.

ACKNOWLEDGMENTS

This work was financially supported by the NSFC (Grant Nos. 21033005 and 21273134) and the National Basic Research Program of China (973 Program, 2009CB930103).

REFERENCES

(1) Jarek, E.; Jasiński, T.; Barzyk, W.; Warszyński, P. *Colloids Surf., A* **2010**, *354*, 188−196.
(2) Hargreaves, W. R.; Deamert, D. W. *Biochemistry* **1978**, *17*, 3759−3768.
(3) Cistola, D. P.; Hamilton, J. A.; Jackson, D.; Small, D. M. *Biochemistry* **1988**, *27*, 1881−1888.
(4) Haines, T. H. *Proc. Natl. Acad. Sci. U.S.A.* **1983**, *80*, 160−164.
(5) Gebicki, J. M.; Hicks, M. *Nature* **1973**, *243*, 232−234.
(6) Namani, T.; Ishikawa, T.; Morigaki, K.; Walde, P. *Colloids Surf., B* **2007**, *54*, 118−123.
(7) Morigaki, K.; Walde, P. *Curr. Opin. Colloid Interface Sci.* **2007**, *12*, 75−80.
(8) Laughlin, R. G. *Colloids Surf., A* **1997**, *128*, 27−38.
(9) Lasic, D. D.; Joannic, R.; Keller, B. C.; Frederik, P. M. *Adv. Colloid Interface Sci.* **2001**, *89−90*, 337−349.
(10) Li, H.; Hao, J. *J. Phys. Chem. B* **2008**, *112*, 10497−10508.
(11) Mcbain, J. W.; Sierichs, W. C. *J. Am. Oil Chem. Soc.* **1948**, *25*, 221−225.
(12) Preston, W. C. *J. Phys. Colloid Chem.* **1948**, *52*, 84−97.
(13) Laskowski, J. S. *J. Colloid Interface Sci.* **1993**, *159*, 349−353.
(14) Yuan, Z.; Lu, W.; Liu, W.; Hao, J. *Soft Matter* **2008**, *4*, 1639−1644.
(15) Long, P.; Song, A.; Wang, D.; Dong, R.; Hao, J. *J. Phys. Chem. B* **2011**, *115*, 9070−9076.
(16) Hao, J.; Hoffmann, H. *Curr. Opin. Colloid Interface Sci.* **2004**, *9*, 279−293.
(17) Song, S.; Zheng, Q.; Song, A.; Hao, J. *Langmuir* **2012**, *28*, 219−226.
(18) Yuan, Z.; Yin, Z.; Sun, S.; Hao, J. *J. Phys. Chem. B* **2008**, *112*, 1414−1419.

(19) Coldren, B. A.; Warriner, H.; van Zanten, R.; Zasadzinski, J. A. *Langmuir* **2006**, *22*, 2474−2481.
(20) Jung, H. T.; Coldren, B.; Zasadzinski, J. A.; Iampietro, D. J.; Kaler, E. W. *Proc. Natl. Acad. Sci. U.S.A.* **2001**, *98*, 1353−1357.
(21) Safran, S. A.; Pincus, P. A.; Andelman, D.; MacKintosh, F. C. *Phys. Rev. A* **1991**, *43*, 1071−1078.
(22) Safran, S. A.; Pincus, P. A.; Andelman, D. *Science* **1990**, *248*, 354−356.
(23) Guida, V. *Adv. Colloid Interface Sci.* **2010**, *161*, 77−88.
(24) Helfrich, W. *Z. Naturforsch.* **1973**, *28c*, 693−703.
(25) Kaler, E. W.; Murthy, A. K.; Rodriguez, B. E.; Zasadzinski, J. A. *Science* **1989**, *245*, 1371−1374.
(26) Brasher, L. L.; Herrington, K. L.; Kaler, E. W. *Langmuir* **1995**, *11*, 4267−4277.
(27) Chiruvolu, S.; Israelachvili, J. N.; Naranjo, E.; Xu, Z.; Zasadzinski, J. A. *Langmuir* **1995**, *11*, 4256−4266.
(28) van Zanten, R.; Zasadzinski, J. A. *Curr. Opin. Colloid Interface Sci.* **2005**, *10*, 261−268.
(29) Coldren, B. A.; Warriner, H.; van Zanten, R.; Zasadzinski, J. A.; Sirota, E, B. *Proc. Natl. Acad. Sci. U.S.A.* **2006**, *103*, 2524−2529.
(30) Israelachvili, J. N.; Mitchell, D. J.; Ninham, B. W. *J. Chem. Soc., Faraday Trans. 2* **1976**, *72*, 1525−1568.
(31) Hervé, P.; Roux, D.; Bellocq, A. M.; Nallet, F.; Krzywicki, T. G. *J. Phys. II* **1993**, *3*, 1255−1270.
(32) Simons, B. D.; Cates, M. E. *J. Phys. II* **1992**, *2*, 1439−1451.
(33) Denkov, N. D.; Yoshimura, H.; Kouyama, T.; Walz, J.; Nagayama, K. *Biophys. J.* **1998**, *74*, 1409−1420.
(34) Coldren, B.; van Zanten, R.; Mackel, M. J.; Zasadzinski, J. A. *Langmuir* **2003**, *19*, 5632−5639.
(35) Egelhaaf, S. U.; Wehrli, E.; Müller, M.; Adrian, M.; Schurtenberger, P. *J. Microsc.* **1996**, *184*, 214−228.
(36) Jung, H. T.; Lee, S. Y.; Kaler, E. W.; Coldren, B.; Zasadzinski, J. A. *Proc. Natl. Acad. Sci. U.S.A.* **2002**, *99*, 15318−15322.
(37) Apel, C. L.; Deamer, D. W.; Mautner, M. N. *Biochim. Biophys. Acta* **2002**, *1559*, 1−9.
(38) Caschera, F.; de la Serna, J. B.; Löffler, P. M. G.; Rasmussen, T. E.; Hanczyc, M. M.; Bagatolli, L.; Bagatolli, A.; Monnard, P. A. *Langmuir* **2011**, *27*, 14078−14090.
(39) Kanicky, J. R.; Shah, D. O. *Langmuir* **2003**, *19*, 2034−2038.
(40) Kanicky, J. R.; Poniatowski, A. F.; Mehta, N. R.; Shah, D. O. *Langmuir* **2000**, *16*, 172−177.
(41) Volkov, A. G.; Paula, S.; Deamer, D. W. *Bioelectrochem. Bioenerg.* **1997**, *42*, 153−160.